

A Review of Speckle Pattern Fabrication and Assessment for Digital Image Correlation

Y.L. Dong¹ · B. Pan¹

Received: 19 September 2016 / Accepted: 3 April 2017 / Published online: 18 May 2017
© Society for Experimental Mechanics 2017

Abstract As a carrier of deformation information, the speckle pattern, or more exactly the random intensity distributions, which could be naturally occurred or artificially fabricated onto test samples' surface, plays an indispensable role in digital image correlation (DIC). It is now well recognized that the accuracy and precision in DIC measurements not only rely on correlation algorithms, but also depend highly on the quality of the speckle pattern. Considering the huge diversity in test materials, spatial scales and experimental conditions, speckle pattern fabrication could be a challenging issue facing DIC practitioners. To obtain good speckle patterns suitable for DIC measurements, some key issues of fabrication methods and quality assessment of speckle patterns must be well addressed. To this end, this review systematically presents the speckle pattern classification and fabrication techniques for various samples and scales, as well as some typical quality assessment metrics.

Keywords Digital image correlation · Speckle pattern · Micro/Nano-scale · Deformation measurement

Introduction

Digital image correlation (DIC), first developed by a group of researchers from the University of South Carolina in the 1980s [1–5], has been continuously refined and widely used in dif-

ferent fields in the past three decades [6, 7]. Due to its incomparable advantages such as simple experimental setup, easy implementation, strong robustness against ambient vibration and light variation, and wide range of applicability with adjustable temporal and spatial resolutions, the DIC technique has been widely accepted as a powerful and flexible tool for shape, motion and deformation measurement for various materials and structures, at diverse temporal and spatial scales, and in different experimental environments.

To illustrate the popularity of DIC techniques, Fig. 1 shows the number of papers retrieved using Web of Science (Science Citation Index Expanded) by inputting <“digital image correlation”>, <“strain gage” or “strain gauge”>, <“moiré interferometry” or “moiré interferometry” > and <“electronic speckle pattern interferometry” > in “topics” respectively in the past 16 years (from 2000 to 2015). It is found that DIC techniques have undergone a burst in methodology research and applications since 2005, which are embodied in the exponentially increased number of publications. In fact, as a representative non-interferometric optical technique, DIC has become more and more popular compared with its interferometric counterparts. Moreover, its popularity in academic publications even exceeds the widely used electrical measurement technique of strain gauge since 2009. It can be said that the DIC method has been and will continue to be the most popular and most important metrology tool in the experimental mechanics community.

Generally speaking, the implementation of DIC techniques for shape, motion and deformation measurements consists of three steps. Namely:

- (1). Speckle pattern fabrication. It ensures the test sample surface has a carrier of deformation information. However, if there is a varying intensity distribution with sufficient contrast on the sample surface, this step can be omitted;

✉ B. Pan
panb@buaa.edu.cn

¹ Institute of Solid Mechanics, Beihang University, Beijing 100191, China

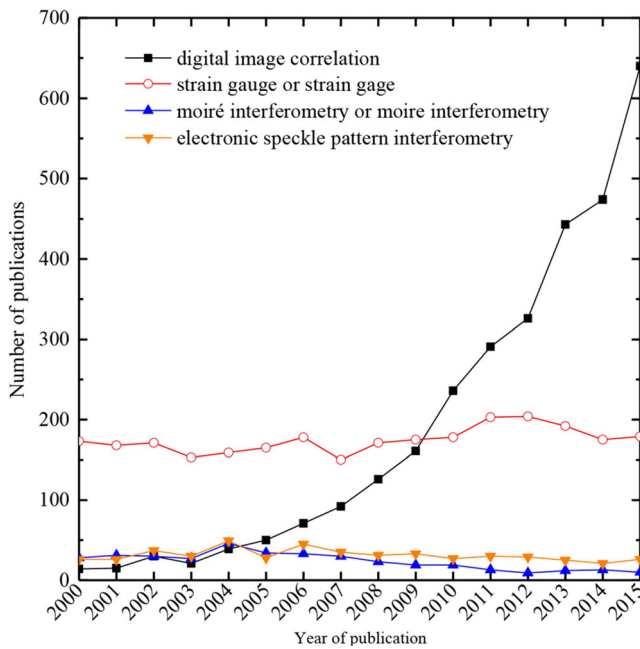


Fig. 1 Number of articles involving typical strain measurement techniques during the past 16 years (from 2000 to 2015)

- (2). Image acquisition. This records the surface images of the test specimen at different states using a single camera (2D-DIC) or two synchronized cameras (stereo-DIC);
- (3). Image analysis. It compares the deformed images with the reference image using a specific cross-correlation algorithm for retrieving displacement and strain fields.

It can therefore be concluded that DIC measurements cannot be realized without the speckle pattern. In other words, the specimen surface must be covered with a speckle pattern (i.e. the random gray intensity pattern), which acts as a carrier of deformation information, to acquire reliable and accurate matching in the subsequent correlation computation. In addition to its indispensability in DIC measurements, speckle patterns also have an important influence on the accuracy and precision in the displacements measurement of DIC. Many researchers have demonstrated [8–21] that a speckle pattern with more plentiful gradients generally leads to smaller bias errors and reduced random errors.

In recent years, DIC techniques have not only seen significant advances in technical development [22–26], but also undergone a burst in applications, ranging from regular metal or polymeric materials to special composite or biological materials [27–31], from macroscopic scale to microscopic scale [32–34], and from common laboratory conditions to extreme environments [35–39]. Speckle patterns can be readily fabricated for most regular experiments where the region of interest has a size ranging from several millimeters to several meters. However, considering the increasing diversity in test materials, spatial scales and experimental conditions, speckle

pattern fabrication and its quality assessment sometimes could be a key challenging issue facing DIC practitioners.

The purpose of this review is to systematically overview the speckle pattern classification, fabrication technique principles and assessment methods, aiming to provide practical guidelines for DIC users. Emphases are placed on the fabrication principles and application examples of speckle patterns in three aspects: (1) with reduced size of micro/nano-scale; (2) at extreme high-temperature environments; (3) involving the field of biomechanics. Moreover, various evaluation metrics of speckle pattern quality are summarized, compared and analyzed. Suggestions for future work are discussed in the conclusion.

What is a Good Speckle Pattern?

As a deformation information carrier, the speckle pattern should have some distinct, unique, non-periodic, and stable grayscale features to realize accurate DIC measurements. Thus, “what is a good speckle pattern?” is undoubtedly a basic but important question, which, in fact, has confused the users of DIC for many years. This part will present several qualitative characteristics (or general guidelines) and a quantitative metric that make a good speckle pattern. Note that the qualitative characteristics are concluded by intuition, while the quantitative metric is derived from solid theoretical error analyses for DIC algorithms.

It should be noted that the speckle patterns created with different methods or by different practitioners may lead to distinctly different histogram distributions, image contrast or other characteristics. To realize accurate DIC measurements, a good speckle pattern should meet several requirements. The speckle pattern on the test sample surface should have: (1) **High contrast**: varying grayscale intensities and relatively large intensity gradients; (2) **Randomness**: non-periodic and non-repetitive pattern to facilitate full field displacement mapping; (3) **Isotropy**: no directionality in the pattern. There should be no obvious directionality in the pattern [40], namely the speckle and the gap between the speckles should be almost the same size in different directions. Speckle granules with a size of 3–5 pixels or slightly greater [41] are highly recommended to avoid aliased effect. (4) **Stability**: a good speckle pattern should tightly adhere to the sample surface and deform with the sample surface together even under large translation and deformation without evident changes in geometric and grayscale characteristics. In a series of short papers written by Phillip Reu [40–44], some key tips and details that help to create a good speckle pattern were discussed from various aspects, such as speckle size (pixels), contrast (grey levels) paint and lighting, speckle edge sharpness (contrast gradient) and speckle density (spatial distribution).

In DIC, the use of the subpixel registration algorithm is regarded as the key technique to improve displacement measurement accuracy and precision. Although different types of subpixel registration algorithms have been developed, the classic forward additive Newton–Raphson (FA-NR) algorithm [45–47] and the recently introduced advanced inverse compositional Gauss–Newton (IC-GN) algorithm [48–51] have been proved to be the two most widely used because of their higher accuracy, wider applicability and better noise-proof performance. Theoretical error analyses of FA-NR algorithm and IC-GN algorithm performed by various researchers now allow us to quantitatively predict the accuracy (bias error) and precision (random error) in the displacements measured. For brevity, Table 1 only lists the corresponding error formula of the two subpixel registration algorithms, derived from the use of the SSD correlation criterion, zero-order shape function and linear intensity interpolation.

It can be seen that no matter by FA-NR or IC-GN, the systematical error $E(u_e)$ and random error $std(u_e)$ are both in inverse proportion to the SSSIG value of the subsets. Theoretically speaking, the speckle pattern that has higher value of SSSIG in the subsets indicates a good speckle pattern [13]. However, one evident shortcoming of SSSIG is that it cannot quantify the randomness of a speckle pattern. In other words, a periodic pattern may have a larger SSSIG value but is not appropriate for DIC analysis. The detailed information about speckle pattern assessment will be presented in Section 5.

Speckle Pattern Classifications

In reviewing the speckle pattern, it is necessary and significant to present its classifications because speckle patterns differ from case to case based on the diverse applications of DIC in various conditions. Natural texture patterns and artificial speckle patterns are generally available in the literature.

However, not much detailed information about the classification of artificial speckle patterns has been presented so far. The purpose of this part is to provide a more detailed classification of speckle pattern.

Natural Texture Patterns

The speckle pattern serving as the information carrier is a key issue in relation to the accuracy and effectiveness in using the powerful tool of DIC. If the sample has good natural texture distribution inherent in its surface, the texture can be used to perform correlation calculation [52]. The deformation monitoring of soil, wood, rocks and other large-scale engineering structures such as bridges can take advantage of the natural texture (e.g., various structures inherent, traffic signs, etc.) for pattern matching [53–55].

In this paper, the natural pattern is defined as the materials' inherent microstructure. The inclusions, grains boundaries, additives, the second phase are all considered as natural patterns. One point should be noted that, the experiment procedure of polishing, scratching or etching are necessary in order to reveal the microstructure of the materials under optical microscopy (OM) or scanning electron microscopy (SEM). This is different from the patterning method of scratching and abrading to make dots or lines on sample surfaces. Table 2 gives a summary of the articles about natural patterns applied in DIC at different image resolutions (The N.A. means information not available). It can be seen sometimes that the natural pattern can be applied for high temperature deformation measurement at low magnification [35, 64, 65]. However, most of the natural patterns are used under SEM or high magnification optical system. The reason is that the microstructure is more clearly seen under high magnification in SEM, scanning probe microscopes (SPM) or high magnification optical system [58, 60–63, 67]. More robust algorithms are prone to be

Table 1 Bias error and random error of FA-NA algorithm and IC-GN algorithm

Subpixel registration algorithm	Bias error	Standard deviation
FA-NR algorithm	$E(u_e) \cong \sum_{i=1}^N \sum_{j=1}^N \left[-h(x_i, y_j) g_x(x_i, y_j) \right] \frac{+(1-2\tau_x)N^2\sigma^2}{\sum_{i=1}^N \sum_{j=1}^N [g_x(x_i, y_j)]} \cdot 2$	$std(u_e) \cong \frac{\sqrt{2}\sigma}{\sqrt{\sum_{i=1}^N \sum_{j=1}^N [g_x(x_i, y_j)]}} \cdot 2$
IC-GN algorithm	$E(u_e) \cong \frac{\sum_{i=1}^N \sum_{j=1}^N [-h(x_i, y_j) f_x(x_i, y_j)]}{\sum_{i=1}^N \sum_{j=1}^N [f_x(x_i, y_j)]} \cdot 2$	$std(u_e) \cong \frac{\sqrt{2}\sigma}{\sqrt{\sum_{i=1}^N \sum_{j=1}^N [f_x(x_i, y_j)]}} \cdot 2$

$h(x_i, y_j)$ is the gray interpolation error at point (x_i, y_j) , $f_x(x_i, y_j)$ the first-order derivative of the grayscale intensities of the reference image, $g_x(x_i, y_j)$ the first-order derivative of grayscale intensities of the deformed image, τ_x subpixel displacement, N the subset size used for calculation, σ the magnitude of the noise, and $\sum_{i=1}^N \sum_{j=1}^N [f_x(x_i, y_j)]^2$ the sum of square of subset intensity gradient (SSSIG) [11]



Table 2 Review of publications involving natural patterns used in DIC

Specimen	Speckle size resolution (μm)	Image resolution ($\mu\text{m}/\text{pixel}$)	Remarks	References
Polymeric foams	N.A	N.A	Robust DIC algorithm, heterogeneous deformation during uniaxial compression	Wang et al. (2002) [56]
Polymer bonded explosives (PBXs)	1	0.5	Optical microscope, sophisticated image cross-correlation algorithm	Rae et al. (2004) [57]
NiTi film	0.01	0.01	Characterizing the nonlinearity of SPM images	Jin et al. (2005) [58]
Al_2O_3	100	N.A.	CCD camera, a robust correlation, coefficient of thermal expansion (CTE)	Srinivasan et al.(2005) [59]
Aluminum, brass, and stainless steel	1	1.3	Light microscopy, distortion removing calibration, displacement/strain	Zhang et al. (2006) [60]
Nickel based LIGA	0.1	0.179	SEM, displacement and strain analysis	Jin et al. (2008) [61]
Compacted graphite cast irons (CGI)	100	1	Stereoscopic camera, microstructural strainfield	Sjögren et al. (2011) [62]
Interstitial free (IF) steel	5	0.2	SEM, large local deformation during in-situ tensile testing	Ghadbeigi et al.(2012) [63]
Cement bauxite	10	97	CCD camera, creep behavior at 1200 °C, four-point bending creep test	Dusserre et al. (2013) [64]
SiC	1000	37.6	CCD camera, an effective grayscale-average technique to minimize thermal disturbance, CTE	Su et al. (2015) [65]
Cancellous bones	N.A	N.A.	Canon camera, formation during indentation test	Xiong et al. (2015) [66]
WB36 steel	1	1	SEM, deformation under uniaxial tension	Zhang et al. (2016) [67]

proposed in using natural patterns to improve accuracy [56, 57, 59, 66] because natural textures are more difficult to do calculation due to the insufficient information carriers or lower quality of texture patterns compared with artificial patterns.

Although microstructures can be used as speckle patterns, it is not easy to find an optimal pattern to warrant accurate DIC matching with relative small subsets. In fact, most of the natural patterns are restricted at micro-scale measurements. Especially, optical and SEM micrographs have been regularly used together with DIC for deformation measurement at micro-scale. However, the procedure to reveal the microstructure with sufficient image contrast is generally considered to be tricky. Therefore most of the speckle patterns are fabricated artificially, which will be analyzed in the next section.

Artificial Speckle Patterns

Different kinds of artificial speckle patterns exist due to different fabrication methods. One often used artificial method is spraying white or black paint by operating a spray bottle or an airbrush to make white or black dots on the sample surface [5, 6]. When the sprayed sample surface is lighted by the illumination of white light [68], or monochromatic light (e.g., blue light [35] or UV light [37]), the random speckle pattern decorated images can be obtained. Laser speckle patterns [69], produced by illuminating the optically rough surface of the sample with a coherent light source (laser beam), have been

used as the carrier of surface deformation information. However, a serious decorrelation effect may occur in laser speckle patterns when the test object is subjected to rigid body motion, excessive straining as well as out-of-plane displacement [70]. That may be the primary reason why laser speckle patterns are rarely used in practical DIC applications.

In this review, the speckle patterns are divided into constructive and destructive types, thus the effect of the fabrication process on the integrity of the original specimen can be clearly known. In the constructive type, spraying and airbrushing are mainly used in macro-scale of millimeters to meters [68, 71], and spin coating, compressed air technique, nano-film remodeling, nanoparticle patterning, focused ion beam (FIB), lithography are applied in micro-scale of micrometers to nanometers [72–76]. In the destructive type, scratching, abrading, chemical etching and FIB milling are mostly utilized in micro-scale pattern fabrication [77, 78]. The detailed information of the fabrication process is presented in the following section.

Fabrication of Speckle Patterns

Different speckle patterns may be accomplished by different operators using the same techniques because the technological parameters play a key role in each technique. In this part, the principles of representative patterning techniques, and the key

parameters in each method are reviewed, meanwhile the application examples are given and analyzed. Detailed information of patterning techniques is summarized to provide a guide in selecting an appropriate technique thereafter.

Airbrushing and Spraying

Macro-Scale Patterns

Airbrushing and spraying is the most common method in fabricating macro-scale patterns. A spray bottle or an airbrush is used. The nozzle diameter, the distance between the substrate and the nozzle, air pressure and viscosity of the solution (as shown in Fig. 2) are important, since they can influence the speckle size distribution and the standard deviation of speckle size distribution [79–81]. Therefore a pre-experiment should be done to determine the parameters.

At room temperature commercial white or black paints are mostly applied as pattern materials [61, 81]. However, at high temperatures, the pattern materials vary according to the measured specimen and temperature applied. Lyons et al. [71] have used BN and Al_2O_3 based ceramic coatings to create a random speckle pattern below 750°C with a speckle pattern size resolution of $100\ \mu\text{m}$ at an image resolution of $25\ \mu\text{m}/\text{pixel}$. Liu et al. [82] have used the same mixture of solution to make speckle patterns applied at elevated temperature of 750°C . Pan et al. [83] have sprayed a mixture of black CoO_2 with high temperature adhesive onto a sample surface that could withstand temperature up to 1200°C with a speckle pattern size resolution of $100\ \mu\text{m}$ at image resolution of $58\ \mu\text{m}/\text{pixel}$. Novak et al. [84] have used Al_2O_3 or ZrO_2 high temperature paints to fabricate speckle patterns applicable at 1500°C with a speckle pattern size resolution of $100\ \mu\text{m}$ at an image resolution of $25\text{--}33\ \mu\text{m}/\text{pixel}$. Pan et al. [85] have made speckle pattern by splashing high-temperature ceramics to the specimen surface. The pattern stranded up to 1550°C without

degradation. Table 3 shows the summary of spraying and airbrushing methods used at elevated temperatures. It can be seen that most of the speckle pattern materials are ceramic oxides because ceramic oxides (Al_2O_3 , ZrO_2 , SiO_2 , etc.) are more stable and heat-resisting at elevated temperatures. Most of the measurements are at macro-scale with image resolution of dozens of micro-meters per pixel (field of view (FOV): dozens of millimeters) [68, 71, 82–95]. The reason is that DIC measurements at high temperatures are more difficult and challenging at micro-scales due to the thermal disturbance induced image noises [37].

Micro/Nano-Scale Patterns

Besides fabricating macro-scale patterns, airbrushing can also create micro-scale patterns. Dong et al. [77] have used airbrush with nozzle sizes of $0.8\ \text{mm}$ and $0.18\ \text{mm}$ to make two kinds of Al_2O_3 patterns on Al_2O_3 substrate. The image resolution of $1\ \mu\text{m}/\text{pixel}$ was reached under microscopy. The fine speckle pattern was proposed to be applied up to 1400°C . Berfield et al. [96] have fabricated a fine, diffused pattern using airbrush with $0.18\ \text{mm}$ of nozzle diameter at a resolution of $10\ \mu\text{m}/\text{pixel}$. Niendorf et al. [97] have used pre-oxidation Si particle as the speckle pattern to characterize the evolution of local strain fields with cyclic deformation at room temperature and 700°C with an image resolution of $2\ \mu\text{m}/\text{pixel}$.

One big potentiality of DIC in biomechanics lies in its suitability to investigate different kinds of materials, such as soft and hard biological tissues, independently of their mechanical behaviors (brittle/ductile, isotropic/anisotropic, homogeneous/inhomogeneous), for small or large deformations. By doing the pressure cycling test of mouse arteries, Sutton et al. [29] have coated toner powder (3 to $10\ \mu\text{m}$ particle size) on the specimen surface to make the speckle pattern to quantify changes in local biomechanical properties in a FOV of $50\ \mu\text{m} \times 250\ \mu\text{m}$. Thompson et al. [98] have studied inhomogeneity of the strain distribution of bone callus of sheep with an image resolution of $7.7\ \mu\text{m}/\text{pixel}$ in a FOV of $23.2\ \text{mm} \times 15.4\ \text{mm}$. The average particle diameter of $8\ \mu\text{m}$ of a photocopier toner mixed into the standard microscopy glycerol gelatin solution was applied to the moist surface of the specimens. A histology brush was used to make the speckle pattern. To measure the tensile properties of the bovine artery, a peripheral coat of black enamel paint was directly sprayed on the surface to generate a high-contrast speckle pattern in a FOV of $25\ \text{mm} \times 100\ \text{mm}$ during the uniaxial tensile experiment [99]. The following Table 4 summarizes examples involving spraying and airbrushing methods in DIC applications in biomechanics.

Studying moisture objects such as biofilm, biotissue and biomaterials under the microscope was one interesting field in biomechanics. Conventional speckle paints and toners show disadvantages such as specular reflections on the moist

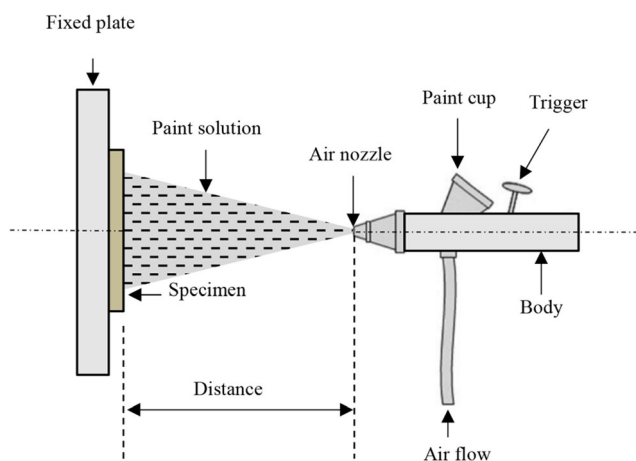


Fig. 2 Schematic illustration of airbrushing method for speckle pattern fabrication

Table 3 Summary of spraying and airbrushing method at elevated temperatures

Sample material	Pattern material	Speckle pattern size resolution (μm)	Image Resolution ($\mu\text{m}/\text{pixel}$)	Temperature ($^{\circ}\text{C}$)	References
6061-T651 aluminum, 304 stainless steel	White and black paint	100	88	600	Turner et al. (1990) [68]
Incoloy 909 and Inconel 718	LSI BN and Al_2O_3 based ceramic coatings	10	25	650	Lyons et al. (1996) [71]
Inconel 800	LSI BN and Al_2O_3 based ceramic coatings	100	32	650	Liu et al. (1998) [82]
Inconel 718	LSI BN and Al_2O_3 based ceramic coatings	100	33	704	Lyons et al. (1998) [86]
Alumina TGO	Al_2O_3 powder (particle size: 0.05 μm) and water mixture	10	N.A.	1200	Sharma et al. (2009) [87]
S235 steel	Black paint on white paint	100	84	600	De Strycker et al. (2010) [88]
1Cr18Ni9T	CoO_2 with an inorganic adhesive	100	58	1200	Pan et al. (2011) [83]
Inconel 625 and C_f/SiC	Aremco Pyro-Paints 634-AL and 634-ZO	100	25–33	1500	Novak et al. (2011) [84]
Al_2TiO_5	N.A.	10	10.9	900	Leplay et al. (2012) [89]
Woven C_f/SiC composite	High-temperature ceramics	1000	N.A.	1550	Pan et al. (2013) [85]
Chromium nickel austenite stainless steel	Black ceramics paints	10	25	600	Pan et al. (2014) [90]
Ti-6Al-4 V	Rustoleum paint	10	N.A.	800	Hammer et al. (2014) [91]
Hastelloy-X	Aremco Pyro-Paint 634-ZO and black Aremco HiE-Coat CM-840)	10	N.A.	1126	Berke et al. (2014) [92]
EBC coated CMC	Y_2O_3 based aerosol paint	N.A.	N.A.	1200	Appleby et al. (2015) [93]
Zirconium silicate	SiC paint	10	16.2	1350	Leplay et al. (2015) [94]
Nickel alloy	Amorphous precipitated SiO_2 and TiO_2 mixture	100	55	1100	Chen et al. (2016) [95]

Table 4 Summary of airbrushing and spraying method in biomechanics applications

Specimen	Patterning method	Field of view (mm × mm)	Imaging resolution (μ/pixel)	Remarks	References
Bovine hoof horn	Airbrushing	6.4 × 8.5	13.3	Tensile test	Zhang et al. (2004) [99]
American lobster (<i>Homarus americanus</i>)	Spraying	2 × 4	0.11	Tensile testing	Sachs et al. 2006 [28]
Mouse tibia	Airbrushing	16 × 12	12	Compression test	Sutton et al. (2008) [29]
Porcine brain tissue	Airbrushing	100 × 125	N.A.	Translational acceleration test	Lauret et al. (2009) [100]
Human vocal ligaments	Airbrushing	6.8 × 8.5	6.7	Tensile test axial strain	Kelleher et al. (2010) [101]
Bovine posterior sclera	Airbrushing	40 × 40	3.4	Inflation test	Myers et al. (2010) [102]
Porcine liver	Airbrushing	80 × 100	3.3	Indentation test	Ahn et al. (2010) [103]
Cortical bone from bovine femoral shaft	Airbrushing	8.7 × 8	17	Three-point bending test	Yamaguchi et al. (2011) [104]
Human liver	Spraying	25 × 25	36	Biaxial tension by inflation test	Brunon et al. (2011) [105]
Acrylic resin mandibular withand without implant	Airbrushing	37.5 × 50	35	Three-point bending test	Tiossi et al. (2011) [106]
Swine brains	Spraying	N.A.	N.A.	Compression tests, relaxation tests and cyclic tests	Libertiaux et al. (2011) [107]
Beaks of granivorous birds	Airbrushing	14 × 17	6.8	Bending test	Soons et al. (2012) [108]
Human skin	Spraying	12.8 × 38.4	50	Tensile test	Ottenio et al. 2014 [109]
Human vertebra	Airbrushing	67 × 100	39	Benchmark test	Palanca et al. (2015) [110]
Aorta of porcine	Airbrushing	18 × 22	3.49	Tensile tests	Zhou et al. (2016) [111]

surface under traditional stereo microscopes with stereo-based DIC. Due to the abundant fluorescent particle size ranging from one nanometer to several microns and excellent biocompatibility with biomaterials, fluorescent particles have been widely used under the fluorescent microscopy combined with DIC. Hu et al. [112] have made a random fluorescence texture pattern by applying a droplet of fluorescent liquid on the sample surface using an airbrush. The use of 3D imaging of the fluorescent micro-particles eliminated the formation of bright parts caused by specular reflections. The recently published technique in improving DIC measurements was called cross polarization which simply consists of placing a linear polarizer between the light source and the specimen and a second polarizer (of a perpendicular polarization axis to the first one) between the specimen and the camera. Thus, the orthogonal polarization between incident and reflected light off the specimen surface selectively attenuated just the specular reflections, resulting in diffuse lighting to the camera. The results showed that cross polarization eliminated saturated pixels that degraded DIC measurements, and increased image contrast, enabling higher spatial precision by using smaller subsets. Also in this work, different speckle pattern sizes were fabricated by an airbrush with 1:1 mixture of methanol and black paint. To create four patterns of different speckle sizes, different pressures were used on four 25 mm × 25 mm quadrants of white-painted areas of super elastic nickel-titanium (NiTi) specimen under uniaxial tension [113].

Though speckle patterns fabricated by spraying and airbrushing are inexpensive and easy-operating, the selection

of proper parameters such as raw material powder size, liquid viscosity, spraying distance and air pressure needs to be determined in advance.

Spin Coating

More than fifty years ago, the pioneering analysis of spin coating was performed by Emsile et al. [114] who have considered the spreading of a thin axisymmetric film of Newtonian fluid on a planner substrate. Spin coating is currently the predominant technique employed to produce uniform thin films of photosensitive organic materials with thickness of the order of micrometers and nanometers [115]. Combined with DIC, spin coating has been developed as a popular method in manufacturing speckle patterns with micrometers and nanometers. The typical stages in making speckle patterns by spin coating are sketched in Fig. 3. It contains deposition, spin-up, spin-off, evaporation solvents and finally the random pattern obtaining. The detailed information can be found in Ref. [116, 117]. Wang et al. [117] have fabricated speckle patterns by spinning a compound of epoxy resin and graphite powder particles through a spin processor. The effect of the proportion of the compound, the spinning rates and the centrifugal solidifying time on the quality of speckle patterns fabricated was studied. The feasibility and accuracy of the fabrication method was proved by deformation measurement of PET thin film and the interface of an optical fiber device.

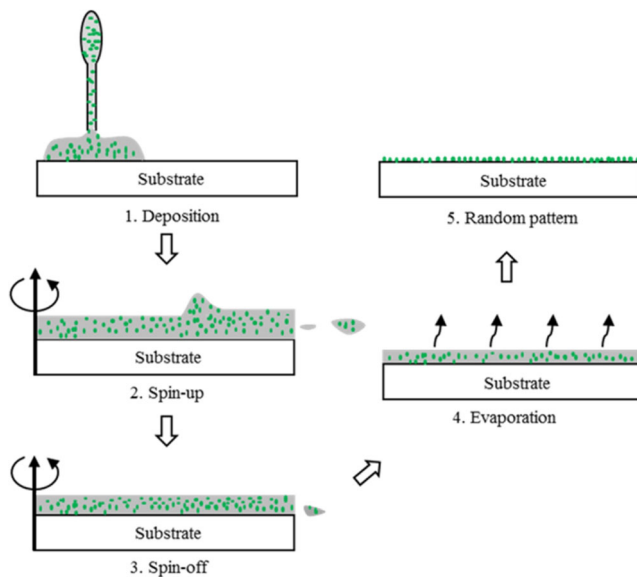


Fig. 3 Typical stages of spin coating process

The full-field measurement of in-plane deformations at scales down to the nano-level has been achieved by fluorescent nanoparticles (c.a. 160 nm in diameter) spin-cast on the top surface of polydimethylsiloxane (PDMS) samples in the work of Berfield et al. [118] in 2006. The resolution was 134 nm/pixel under a compound fluorescent microscope in a FOV of $171 \mu\text{m} \times 137 \mu\text{m}$. The fluorescent speckle pattern created by the excitation of rhodamine dye infused silica nanoparticles (140 to 180 nm in diameter) solution deposited onto the polymer sample surface by spin coating has been conducted by Berfield et al. [96]. The displacement accuracy of 17 nm was accomplished via DIC measurement through rigid body translation and uniaxial tensile testing. The fluorescence imaging can avoid unwanted specular reflections of moist surface and heat induced by white light to change the investigation environment. The in-plane strain development within lead zirconate titanate (PZT) sol-gel thin films subjected to thermal loading was measured using a fluorescence-based DIC method by Berfield et al. [119]. Fluorescent silica nanoparticles with a final diameter of about 140 nm was spin-coated on the sample surface as the speckle pattern in a $200 \mu\text{m} \times 200 \mu\text{m}$ area. Hamilton et al. [120] have studied the mechanical behavior of epoxy-matrix microvascular networks loaded in tension using fluorescent digital image correlation technique. The speckle pattern was made by spin-coating fluorescent silica nanoparticles on the order of 300 nm. By spin-coating fluorescent nanoparticles on a carbon fiber composite specimen and an aluminum control specimen, Wilhelmsen has studied the evolution of highly localized displacements and strains of the specimens under transverse tension [121].

Due to the maturity of research in literature, a low cost and fast operating system, spin coating has a great potential in

speckle pattern manufacturing ranging from nanometers to micrometers. However, large substrate cannot be spun at a sufficiently high rate in order to allow the film to thin.

Compressed air Technique

Jonnalagadda et al. [75] firstly used the compressed air technique to make micro-scale speckle patterns. Figure 4 shows the schematic of the compressed air technique. There is a hollow cylindrical shaft with side inlets to introduce compressed air at the bottom of the cylinder and micro-scale particles above the air inlet. The powder is blasted through three filters to eliminate large agglomerated particles. The dies with Pt specimens are placed at the top of the cylinder in an inverted position to collect the particles forced by the compressed air through the topmost filter. Micro-particles adhere onto the freestanding specimens by Van der Waals forces and static charges. The filtration fineness (the maximum size of escaping particles) of filters I-III, filtering time and raw powder size can be tuned to obtain the optimal pattern.

Using this method, Si pattern has been accomplished by depositing $1 \mu\text{m}$ diameter Si particles on the polycrystalline metal specimen surface with a resolution of $0.087 \mu\text{m}/\text{pixel}$ in a FOV of $92 \text{ pixels} \times 92 \text{ pixels}$ [122]. Karanjgaokar et al. [123] have conducted a tensile experiment of Au films. Full-field strain measurements were done using submicron sized speckle patterns made by the compressed air technique at 110°C . $1 \mu\text{m}$ silicon particles have been patterned on the surface area of zirconium grade 702 (Zircadyne) with a resolution of $1.2 \mu\text{m}/\text{pixel}$ by Padilla and his collaborators [124]. Recently, Casperson et al. [125] have investigated the fatigue crack growth and crack closure of Hastelloy X up to 650°C with 1 to $5 \mu\text{m}$ silicon particles. Pataky et al. [126] studied the heterogeneous strain fields of Haynes 230 using DIC. With the $0.3 \mu\text{m}$ alumina powder, the speckle pattern was accomplished by this method with a digital image resolution of $0.175 \mu\text{m}/\text{pix}$ up to 800°C .

Although the pattern consistency can be achieved without worrying about having random large speckles, as seen with spraying paint, and the large range of materials available to

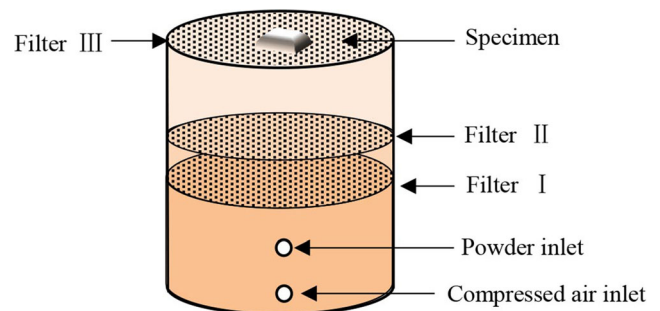


Fig. 4 Schematic of compressed air technique in fabricating speckle patterns [75]

deposit, the adherence of particles to the surface should be considered with this method because the micro-particles adhere onto the freestanding specimens by Van der Waals forces and static charges. Moreover, at a higher temperature (for example above 1000 °C), the stability of the pattern on the substrate surface has to be taken into account and needs more studies.

Nano-Film Remodeling

A promising pattern application method for producing the desired high-density speckle patterns is vapor-assisted remodeling of deposited metal films. Luo et al. [127] have studied the remodeling of ultrathin (<20 nm) gold films by exposure to condensable vapors of volatile solvents systematically for the first time. It was proposed that the metal film morphology could be controlled by the choice of the initial film thickness, exposure time, and substrate temperature. A theoretical model for capillary condensation capturing the essential elements of the vapor-assisted remodeling mechanism was adapted. The schematic set-up is shown in Fig. 5. The metal-coated slide is mounted on a slide holder which also serves as a heater with calibrated temperature control. The chemical vapor flows into the flask from a front pressure valve and passes out of the flask through a back pressure valve.

Using this method, Scrivens et al. [128] have successfully fabricated patterns onto polymeric and metallic materials ranging from 50 to 500 nm. The effect of exposure time, coating thickness, temperature and chemical vapor type were studied and analyzed. The gold pattern maintained adherence to the polymer specimen throughout the straining process. These results indicated that the embedded pattern in the polymer substrate had the potential for use with digital image correlation and imaging via an environment scanning electron microscope (ESEM) or similar imaging system to make deformation measurements with sub-micron spatial resolution. Li et al. [129] have applied a layer of gold on aluminum slides with vapor-assisted remodeling. The feature size was

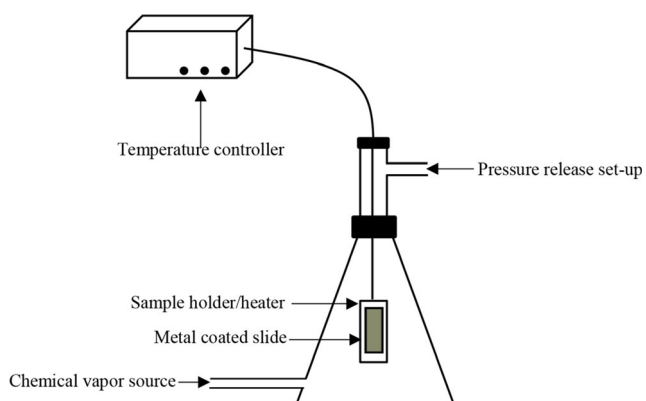


Fig. 5 Schematic set-up of metal film remodeling

100 to 150 nm. The effectiveness of the speckle pattern was verified by measuring the thermal strain of AL-2024-T3 using SEM-DIC. Recently, Di Gioacchino et al. [130] have developed a new set-up to make gold patterns by vapor-assisted remodeling. The nano-scale speckles were of size ranging from 30 to 150 nm and of similar spacing in sub-regions ranging between approximately 100 nm × 100 nm to 300 nm × 300 nm. The deformation fields at the scale of slip bands of 304 L stainless steel during the tensile experiment showed the potential of the vapor-assisted remodeling technique.

The nano-film remodeling has the advantage of particle morphology controlling and reproducing. However, it is time consuming in two steps. The nano-film has to be coated on sample surface as the first step. Moreover, different nano-film coating methods can also have an effect on the formed speckle pattern which has not been reported in detail.

Lithography

E-beam lithography technique (EBL) or UV lithography technique is mostly used to manufacture IC (Integrated Circuits) chips and micro-scale devices [131, 132]. In DIC, combined with high magnification imaging techniques (SEM, STEM, AFM), lithography is used to generate micro/nano-scale random patterns on the specimen surface to understand the effect of microstructure (grain boundaries, second phases, defects, etc.) on the macroscopical response of materials [133–135]. Figure 6 shows the schematic steps in obtaining speckle patterns by e-beam lithography. After polishing and cleaning the substrate surface, the resist of PMMA is spin-coated on the substrate surface in Step one, then the resist is irradiated by focused electron beam in the electron exposure step, and then the irradiated portions of the resin are dissolved in Step three. Metal or dielectric is deposited over the entire surface as shown in Step four. Finally, the remainder of the resin is developed and thus the deposition is left as the speckle pattern. More details can be found in Ref. [136, 137].

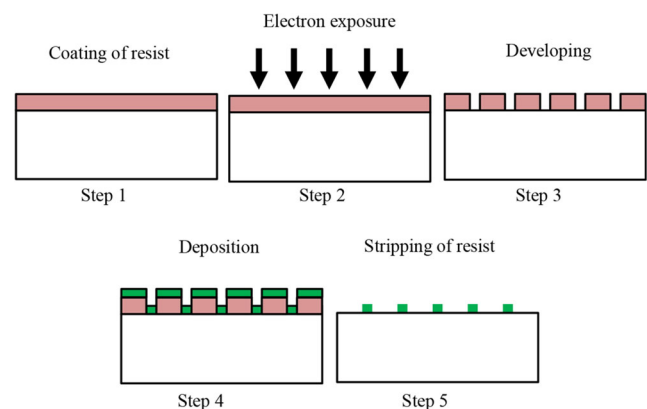


Fig. 6 Schematic diagram of the e-beam lithography steps (one-five)

Li et al. [138] have fabricated random patterns ranging from 150 nm to 500 nm on Al and Si specimens using ELT. The LabView software was written to control the e-beam motion process to greatly reduce the time for etching a dual-layer photo-resist coating. Tanaka et al. [139] have utilized e-beam lithography to make random patterns for micro/nano-scale measurements by backscattered electron imaging (BSEI) under field emission SEM. Scrivens et al. [128] have made gold and silver or other metal patterns with 2 to 20 μm by UV photolithography through a large amount of laboratory preparation. The adherence of the sputtered random pattern of tantalum to the surface of AA 8009 aluminum alloy was verified by the fatigue test.

According to the heat resistant properties of the pattern material, speckle patterns used at elevated temperatures are also an interesting field under research. Walley et al. [72] have deposited hafnium oxide on nickel-base superalloy Rene 104 to make a speckle pattern by e-beam lithography. The pattern was between 0.45 and 0.7 μm incorporating a set of alphanumeric markers every 200 μm to help facilitate locating particular regions within the 0.01 cm^2 analysis area after testing. It proved that the pattern had good thermal stability and provided excellent contrast for image acquisition using secondary electron imaging at an elevated temperature up to 700 $^\circ\text{C}$. Carter et al. [140] have conducted hafnium oxide on the sample of nickel-based superalloy of Rene-104 using ELT. In their studies, how the patterning parameters (speckle density and shape) affected the strain resolution of DIC using SEM imaging was analyzed. The plastic deformation distribution at a constant stress with heating up to 700 $^\circ\text{C}$ was assessed.

Although ETL is substrate independent, repeatable and designable, the disadvantages of e-beam lithography are its high cost and limited applicability to non-flat substrates due to its sensitivity to working distance. In addition, it is time assuming and expensive.

Focused ion Beam (FIB)

The focused ion beam (FIB) technique was mainly developed during the late 1970s and the early 1980s [141]. Recently, the FIB milling and deposition have been developed combined with SEM applied in DIC for deformation measurements at micro-scale [142, 143]. The pattern generation principle with FIB milling is shown in Fig. 7(a). Removal of sample materials is achieved using a high ion current beam. Sebastiani et al. [144] have fabricated periodic holes as speckle patterns for nano-scale measurements by FIB milling. By scanning the beam over the substrate, an arbitrary shape can be etched, Li et al. [145] have developed speckle patterns on the surface of silicon wafer and amorphous silicon carbide by FIB milling. Their study shows that in design of speckle patterns selecting a best template and a proper magnification of FIB were

essential. The influencing factors including etching time and ion beam current were also discussed.

Figure 7 (b) shows the schematic of FIB deposition. The precursor gas flows on the surface of the sample with the help of a gas jet, and it gets adsorbed on surface molecules. When the ion beam hits the sample surface it decomposes the adsorbed precursor gases. The volatile reaction products come out from the surface and are removed through the high-vacuum system, and the desired reaction products remain on the sample surface as a thin film. Sabate et al. [146] have acquired speckle patterns by the deposition of a 20 nm Pt layer with FIB for nano-scale measurement. Winiarski et al. [147] have compared patterning methods of YSZ nanoparticles, FIB assisted Pt dots and FEB Pt dots in their paper. It is proposed that the FIB assisted decoration technique has the advantage of rapid processing time and tolerant processing conditions, however, it has a concern with surface damage due to ion implantation. Recently, Zhu et al. [148] have considered the influencing parameters such as the quality of the speckle template, total deposition time, ion beam current density, and dwell time on the deposited speckle pattern. The residual stress distribution on the laser shock peened metallic glass surface was successfully measured to verify the effect of the pattern

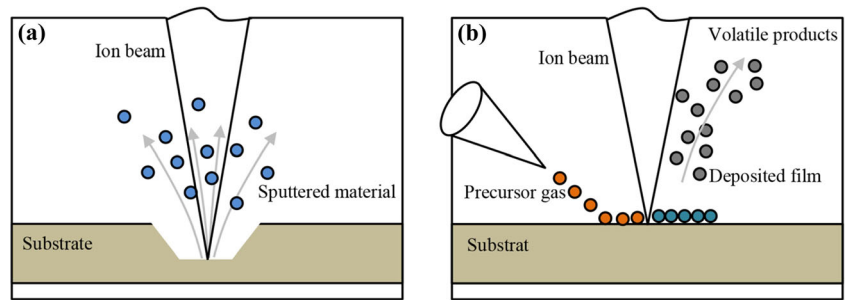
Although the FIB patterning method is repeatable, substrate independent and speckle pattern location controllable, it is expensive and sample surface damaging.

Scratching and Abrading

Besides the methods presented above involving adding materials to the sample surface to form speckles, taking materials from the sample surface including scratching, abrading is also used in fabricating speckle patterns.

Grant et al. [35] have abraded the surface of the alloy using silicon carbide paper to obtain the speckle pattern with a 10 μm speckle size resolution at an image resolution of 2.5 $\mu\text{m}/\text{pixel}$ to measure the Young's modulus and CTE up to 800 $^\circ\text{C}$. Dong et al. [37] have measured the CTE of polycrystalline Al_2O_3 up to 1400 $^\circ\text{C}$ using scratches of 1 μm speckle resolution as the speckle pattern with an image resolution of 1 $\mu\text{m}/\text{pixel}$. Thompson et al. [149] have measured the thermal expansion of a Rene N5 superalloy and NiCoCrAlY bond coat alloy up to nearly 1100 $^\circ\text{C}$. A piece of 20 Pm diamond paper was utilized to produce a subtle scratch pattern on the surfaces. Blaber et al. [150] have sandblasted the sample surface with an average particle size of 500 μm and subsequently laser etched with an infrared laser engraving to make speckle particles of about 50 μm on PWA1484. The stability of the surface pattern was verified through two load cycles of ~ 20 min each at 1000 $^\circ\text{C}$ during a single edge notched tension test.

Fig. 7 Schematic illustrations of (a) FIB milling and (b) FIB deposition



Scratching or abrading techniques are simple, inexpensive, do not need pattern materials and can make both macro/micro-size patterns. Measurements can also be done at elevated temperatures based on the sample materials. However, the surface will be damaged and residual stress can be induced. Moreover, it will be a waste of specimen once failure in scratching or abrading occurs.

Other Techniques

In addition to the techniques presented above, among constructive methods, the permanent marker, stamp, temporary tattoo, India (calligraphy) ink, carbon printer toner and graphite powder, microsphere fiducial markers, etc. are also used for macroscopic scale patterns and micro-scale pattern fabrication [151–165]. Helm et al. [154] have analyzed the multiple, growing cracks of a slab of reinforced concrete with 2100 mm × 2100 mm subjected to a uniformly distributed pressure load. The speckle patterns used were small felt disks, similar to those used to cushion the bottom of furniture legs. The dots in the local image area were approximately 10 mm in diameter which corresponded to a dot diameter of approximately 8 pixels in the images. 3D bone ligament-bone (BLB) and native medial collateral ligament (MCL) samples under cyclic tension loading have been tested via DIC using blue microsphere fiducial markers with a 25 mm diameter brushed on the surface as speckle pattern [155]. Avitabile et al. have measured the mode shape of an aluminum structure with 609 mm × 914 mm in size via DIC with a black permanent marker creating the speckle pattern on flat white spray paint coating the areas [156]. In order to prepare helmets for DIC testing for back face deformation, ink tattoo has been utilized as the speckle pattern [158]. By tracking the black India ink on the cylindrical surface of the cartilage sample, the average nominal strain was measured by Deneweth et al. [161]. Mahalingam et al. [162] have had graphite powder blown onto the specimen of anterior cruciate ligament (ACL) and BLB of adult Black Suffolk sheep to create a surface pattern for uniaxial tension tests.

Combined with SEM, the grid method has been used for speckle patterning method in the microscale deformation characterization. Biery et al. [151] have measured strains at the scale of the microstructure of gamma-TiAl alloys. The polished samples were gridded by evaporating gold through

a 1500 line-per-inch nickel mesh as the speckle pattern. Biery et al. [152] have measured the local straining in γ -titanium aluminides using gridding by evaporating gold onto the sample surface through fine nickel grids of 1500 lines per inch. For a higher resolution combined with SEM, the nano-scale speckle pattern has been fabricated by Kammers et al. [160] using an AuNP self-assembly technique. By adjusting technical parameters, the patterns with speckle sizes ranging from tens of nanometers to hundreds of nanometers were created.

Brief Summary

Artificial techniques of spraying and airbrushing are inexpensive and can be easily operated. For ordinary testing conditions such as tensile, compressive experiments at room temperature and elevated temperatures, this patterning technique is recommended. Micro/nano-scale speckle patterning techniques including spin coating, compressed air technique, nano-film remodeling, FIB and lithography are mainly used for the high magnification optical microscopes, SEM, AFM, etc. Scratching/abrading is simple and easily operable, but is surface damaging. Spin coating, compressed air technique and nano-film remodeling are potential techniques due to their low cost and high efficiency. FIB and lithography are usually expensive and time consuming. The detailed summary of the patterning methods are shown in Table 5.

Speckle Pattern Assessment

Patterns fabricated using different techniques by different operators may have different qualities. Quality assessment metrics have been proposed as a series of parameters in literature. A common practice is to divide into the local and global parameters. This section will summarize the existing metrics for the assessment of the speckle pattern quality.

Local Parameters

Local parameters aim to quantify the speckle pattern with individual subsets and are expected to help with the optimal

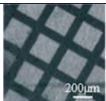

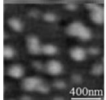
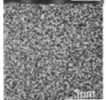
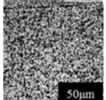
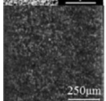
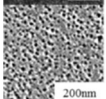
Table 5 Summary of artificial pattern techniques

Patterning method		Imaging system	Typical image	Feasible speckle size range	Initial cost	Production cost	Estimated time start to finish	Process scalability	References
Constructive	Spraying	OM, OC		1 to 1000 μm	Inexpensive	Inexpensive	Minutes to hours	Moderate	[2, 45]
	Black permanent marker	OM, OC		100 μm and up	Inexpensive	Inexpensive	Minutes to hours	Moderate	[156]
	Microstamp/Stamp	SEM, OM, OC		1 to 1000 μm	Moderate	Inexpensive	Minutes to hours	High	[154, 165]
	India (calligraphy) ink	OM, OC		100 μm and up	Inexpensive	Inexpensive	Minutes to hours	High	[158, 161]
	Carbon printer toner and graphite powder	SEM, OM, OC		1 to 100 μm	Inexpensive	Inexpensive	Minutes to hours	High	[5, 153, 157, 162]
	Airbrushing	OM, OC		1 to 1000 μm	Moderate	Inexpensive	Minutes to hours	Moderate	[99-104]
	Spin coating	SEM, OM, OC		1 to 1000 nm	Moderate	Inexpensive	Minutes to hours	Moderate	[96, 118-121]
	Nanoparticle patterning	SEM, OM		1-100 nm	Moderate	Inexpensive	Minutes to hours	Moderate	[73]
	Self-assembled nanoparticles	SEM, OM		1-1000 nm	Moderate	Inexpensive	Days and up	High	[160]
	Compressed air	SEM, OM		1 to 1000 nm	Moderate	Moderate	Hours to days	Moderate	[75, 123-127]
	Microsphere fiducial markers	SEM, OM		1 to 100 μm	Inexpensive	Inexpensive	Minutes to hours	Moderate	[155, 164]
	Nano film remodeling	SEM, OM		1 to 1000 nm	Expensive	Expensive	Hours to days	Low	[74, 127-130]
	E-lithography	SEM, OM		1 to 1000 nm	Expensive	Expensive	Hours to days	Low	[128, 133-140]
	Photolithography	SEM, OM		1 to 100 μm	Moderate	Moderate	Minutes to hours	Moderate	[5]

selection of subset sizes. Various local parameters have been proposed and their definitions are listed in Table 6, including subset entropy presented by Sun et al. [10], mean subset fluctuation by Hua et al. [14] and SSSIG by Pan et al. [11]. Note that the parameters of subset entropy and mean subset

fluctuation are related to SSSIG to some extent. For example, by defining $|\nabla f(x_i, y_i)| = \sqrt{f_x(x_i, y_i)^2 + f_y(x_i, y_i)^2}$ (where $f_x(x_i, y_i)$ and $f_y(x_i, y_i)$ are the first derivatives of the intensity gray value of $f(x_i, y_i)$ at pixel coordinate (x_i, y_i) and carefully

Table 5 (continued)

Constructive	Template patterning with TEM grid	SEM,OM		1 to 1000 nm	Moderate	Moderate	Minutes to hours	High	[151, 152, 159]
	Temporary tattoo	OM, OC		1000 µm and up	Inexpensive	Inexpensive	Minutes to hours	Moderate	[158, 163]
	FIB deposition	SEM,OM		1 to 1000 nm	Expensive	Expensive	Hours to days	Low	[76, 146-148]
Destructive	FIB milling	SEM,OM		1 to 1000 nm	Expensive	Expensive	Hours to days	Moderate	[144, 145]
	Scratching	OM, OC		1 to 100 µm	Inexpensive	Inexpensive	Minutes to hours	Moderate	[37, 149]
	Abrading	OM, OC		1 to 100 µm	Inexpensive	Inexpensive	Minutes to hours	Moderate	[35]
	Chemical etching	OM, OC		1 to 100 µm	Moderate	Moderate	Hours to days	Low	[78, 150]

choosing the discrete estimations of the derivatives, the two metrics are equivalent of subset entropy and SSSIG, save for a scaling term. However, it should be noted that subset entropy and mean subset fluctuation are derived empirically without solid theoretical basis, while SSSIG is an outcome of substantial theoretical error analysis performed for subpixel registration algorithms.

As given in Table 1, theoretical error analysis of the classic FA-NR algorithm and the state-of-the-art IC-GN algorithm performed by different research groups [45–51] all revealed that both the accuracy and precision of the measured displacements are inversely proportional to SSSIG. For this reason, SSSIG has been considered as the most effective and widely adopted local parameter for quantitative quality assessment of speckle patterns within a single subset [13, 21]. It is worth noting that, since the precision of DIC measurements can be accurately predicted by the known noise level of the image as well as SSSIG [11], Pan et al. further proposed a method for the optimal selection of subset size by adjusting SSSIG to preset values to suppress the adverse influence of image noise. The same idea has also been extended to subvolume size selection [167] for internal displacement field analysis using digital volume correlation.

Although SSSIG is a rigorous metric for local speckle pattern quality evaluation, it still has two limitations. First, SSSIG cannot differentiate random speckle patterns and periodic patterns. In other words, periodic patterns such as the checkerboard may have high SSSIG values, however, it cannot be

considered as an effective pattern for DIC analysis. Second, as a local parameter to assess the quality of each subset separately, SSSIG is limited to the quality assessment of the local speckle pattern within an individual subset. However, for most isotropic speckle patterns with evenly distributed speckle granules, the local parameters computed for various subsets are normally of very little difference. For this reason, several global parameters have been developed in the literature.

Global Parameters

In addition to local parameters, various global parameters have been proposed to quantify the entire speckle pattern. In this respect, Zhou and Goodson first [8] proposed that high quality patterns should be with of speckle sizes from 2 to 5 pixels through numerically simulated speckle patterns consisting of discrete Gaussian granules. Following the idea of Zhou et al., Lecompte et al. [9] used an image morphology method to determine the mean speckle size of a speckle pattern. The mean speckle size in combination with the subset size had an influence on the accuracy of the measured displacements. Hung et al. [166] used an averaging technique to assess the pattern. However, for these global parameters, the threshold method in edge detecting to determine speckle size would miss the true edge of shapes in patterns.

Pan et al. [13] refined the local parameter SSSIG to evaluate the quality of the entire speckle pattern by developing a

Table 6 Summary of speckle pattern assessment parameters

Pattern assessment criteria	Global or local	Remarks	Disadvantage	Remarks	References
Subset entropy $\delta = \frac{\sum_{i=0}^8 I_i P_i - I_i}{2^{\beta} MN}$	Local	An indication of the fluctuation, or “randomness”	Not showing variation between subsets in the pattern	δ is subset entropy, P any pixel point in a subset S with it size $M \times N$, I_i the intensity at point P , I_i the intensity at one of 8 pixel points neighboring point P , β the depth of an image, for 8 bit image (β is 8).	Sun et al. (2007) [10]
Sum of square of subset intensity gradients	Local	Capable of detecting the proper subset size	Not showing the variability within the pattern		Pan et al. (2008) [11]
SSS(GSSSIG) $= \sum_{i=1}^N \sum_{j=1}^N \left[\int_{x,y} f(x,y) \right]^2$	Local	Showing speckle size from 2 to 4 pixels and large density preferred	Not showing variation between subsets in the pattern	a_{ij} is the gray value of each point, \bar{a} is the mean gray value of the subset, P point in the subset, F the class of the points,	Hua et al. (2011) [14]
Mean subset fluctuations $S_f, S_f = \frac{\sum_{i \in P} \sum_{j=1}^3 \sum_{k=1}^3 a_{ij} - \bar{a} }{H \times V}$	Local			$H \times V$ the size of the speckle pattern.	Zhou et al. (2001) [8]
Speckle size	Global	Optimal speckle size of 2 to 5 pixels preferred	Missing the true edge of shapes in patterns by threshold method		Hung et al. (2003) [166]
Average speckle size	Global	Relatively small consumption of the computational time	Missing the true edge of shapes in patterns by threshold method		Lecompte et al. (2006) [9]
Morphological methodology	Global	Showing effect of size of the speckles combined with the size of subset	Missing the true edge of shapes in patterns by threshold method		
Mean intensity gradient	Global	Showing large mean intensity gradient preferred	Not showing variability within the pattern	$\nabla f(x_{ij}) = \sqrt{f_x(x_{ij})^2 + f_y(x_{ij})^2}$ is the modulus of local intensity gradient vector with $f_x(x_{ij}), f_y(x_{ij})$ which are the x and y -directional intensity derivatives at pixel (x_{ij}) , W and H (in unit of pixels) image width and height.	Pan et al. (2010) [13]
MIG $\delta_f = \sum_{i=1}^W \sum_{j=1}^H \left \nabla f(x_i, y_j) \right / (W \times H)$	Global				
Comparison parameter q of main and secondary autocorrelation peak $q = \frac{C_{max} - C_{sec}}{S(C)}$	Global	Quantitative evaluation of random patterns through comparing primary and secondary peaks	Not ideal for normalization of the difference between primary and secondary peaks	C_{max} is the main peak value, C_{sec} the secondary peak value of the cross-correlation function, $S(C)$ standard deviation of the cross correlation function value.	Stoilov et al. (2012) [15]
Morphological methodology	Global	Showing even distribution of speckle sizes preferred	Not showing randomness of pattern		Crammond et al. (2013) [16]
Autocorrelation peak sharpness radius $R_{peak} = \sqrt{\frac{A_{\beta} - A_0}{(A_{\beta+1}) - A_0}}$	Global	Quantitatively evaluating deformation sensitivity of pattern	An optimal value of the quality metric leading to a non-optimal DIC pattern	A_0 is the autocorrelation value for zero displacement, $A_{\beta+1}$ mean of the autocorrelation values for displacements by 1 pixel, A_{β} the parabolic peak shape to the autocorrelation value for full-contrast random noise.	Bossuyt et al. (2013) [17]
Shannon entropy $H(Y) = - \sum_{i=0}^{2^{\beta}-1} p(a_i) \log(p(a_i))$	Global	Large Shannon entropy preferred	Not showing changes in fundamental features of the stochastic pattern	H is Shannon entropy, bits/pixel, β the pixel depth of the image (the 8-bit image is used in actual practice, that is $\beta = 8$, $p(a_i)$ the normalized probability of the occurrence of each gray level, which can be computed by the histogram of the image.	Liu et al. (2015) [18]
Speckle distribution and speckle size range	Global	Showing an even speckle size distribution and wide speckle range preferred	Missing the true edge of shapes in patterns by threshold method		Dong et al. (2015) [77]

Table 7 Numerical comparison of assessment metrics

Assessment metric	Global or local	1#	2#
MIG, δ_f	Global	28.48	16.68
Autocorrelation peak sharpness radius, R_{peak}	Global	2.96	5.56
Main and second autocorrelation peak comparison, q	Global	0.28	0.29
Shannon entropy, H	Global	5.25	5.18
SSSIG	Local	825.86	483.78
Mean subset fluctuation, S_f	Local	184.71	108.66
Subset entropy, δ	Local	0.23	0.14

global parameter called the mean intensity gradient (MIG). Numerical experiments have shown that a speckle pattern with the larger MIG produces smaller mean bias error and standard deviation error. Hence, a good speckle pattern should be of large MIG. The MIG for speckle pattern quality assessment can be used for at least the following three purposes in DIC measurements: (1) it can be used as the guidance for practical sample surface preparation; (2) it can be used to predict the precision of the measured displacements; (3) combined with the desired displacement measurement precision, it can be used for subset size selection for various speckle patterns.

Liu et al. [18] have proposed Shannon entropy to assess pattern quality through measures of the information content of an image and considered that a good quality speckle pattern should have a large Shannon entropy. An autocorrelation peak sharpness radius R_{peak} of a pre-processed image of the pattern has been proposed by Bossuyt et al. [17] to quantitatively evaluate how a particular pattern influences the sensitivity of a DIC measurement. Patterns with more features, higher contrast and sharper edges have a smaller autocorrelation peak sharpness radius, corresponding to better displacement sensitivity in DIC measurements. However, an optimal value of the quality metric can lead to a non-optimal DIC pattern taking an checkerboard pattern with single pixel squares as an example. Stoilov et al. [15] have proposed a metric based on the comparison of the variation of primary and secondary peaks during deformation. However, normalization of the metric is not ideal because a pattern with a single large secondary

auto-correlation peak would have worse quality than a pattern with many large secondary auto-correlation peaks. Crammond et al. [16] have proposed that global parameters such as MIG are not in themselves sufficient to evaluate strain accuracy. In their studies, the global parameter Shannon entropy [18] which measures the information content was compared with the morphological technique. The Laplacian of Gaussian edge detection method was used to identify the individual speckles. The numerical experiment showed that the most even distribution of speckle sizes in the morphological assessment resulted in the lowest errors. The conclusion well matched the result described by Dong et al. [77]. A review of the local and global pattern assessment metrics is shown in Table 6.

Numerical Comparison of Various Assessment Metrics

To compare these assessment metrics, a numerical analysis was conducted using two speckle pattern images. A high contrast pattern image was selected from the well-recognized round robin study (<https://sem.org/dic-challenge/>) as shown in Table 7, 1# speckle pattern image. 2# speckle pattern image shown in Table 7 was generated using Matlab software (R2016a). The assessment parameters were calculated as shown in Table 7. It shows that 1# pattern had a larger value of δ_f , SSSIG, S_f , δ , the same value of q and H , a smaller value of R_{peak} , compared with 2# pattern (subset size used was 29 pixels \times 29 pixels for calculating local parameters).

Numerical translations were exerted to the two reference images with 0.1 pixel shifting from 0 to 1 pixel in x direction. The displacement was measured using IC-GN algorithm with zero-normalized sum of squared difference (ZNSSD) correlation criterion [48], first-order shape function and cubic B-spline interpolation. Totally, 5640 points were calculated with a subset size of 29×29 pixels and a grid step of 5 pixels. The mean bias error u_e and standard deviation error σ_u of measured displacement u , whose definition can be found in Ref. [13], are shown in Fig. 8. It can be seen that 1# pattern image had both smaller mean bias error and standard deviation error compared with 2#. This indicates that 1# pattern had higher quality which well agreed with the larger value of δ_f , SSSIG, S_f and δ as shown in Table 7. Since S_f and δ are related to SSSIG to some extent [21], as a result, SSSIG can be esteemed most strongly correlated to DIC accuracy and precision [21].

Brief Summary

Both local and global metrics for speckle pattern quality assessment have been overviewed and quantitatively analyzed using numerical translation tests. Among these parameters, SSSIG and MIG have been esteemed as the most effective local and global metrics with solid theoretical foundations [13, 21]. However, these two metrics cannot be used to assess the randomness in a speckle pattern. For this reason, we consider that no single existing parameter can be a decisive measure for the pattern quality assessment [16]. In reality, the potential perfect way in assessing and optimizing speckle patterns should be based on an integrated metrics, which combines SSSIG with other parameters that can quantify the randomness of speckles. Recently, Bomarito et al. [21] suggested a new pattern quality metric which is based on a linear combination of three individual metrics (i.e., the SSSIG, watershed radius and secondary auto-correlation peak height). They used the combined pattern quality metric to generate optimal patterns, based on which DIC

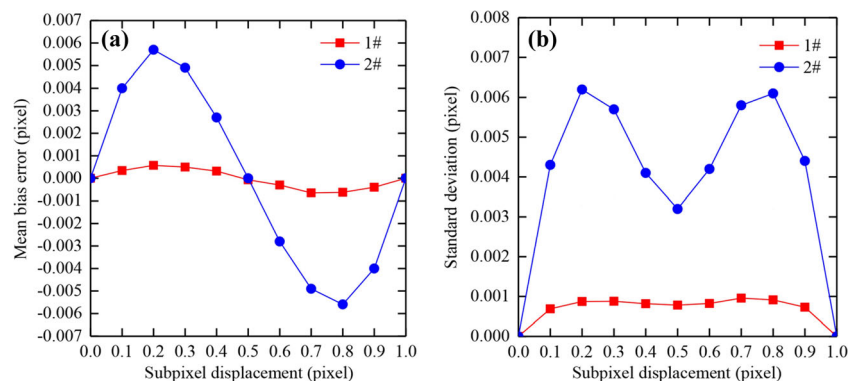
measurements are demonstrated with increased accuracy and precision in numerical and real experiments.

Conclusion

As an indispensable issue in using DIC, the speckle pattern is closely related to the accuracy and precision of DIC measurement. In this review, for the first time, the classification, fabrication and quality assessment of speckle patterns are comprehensively reviewed along with typical application examples. Emphases are specially placed on fabrication principles and application examples of speckle patterns in three aspects: those applied at extreme environment of elevated temperatures, those with reduced size of micro/nano-scale fabrication, and those in the field of biomechanics. The quality assessment metrics for speckle patterns are summarized and commented in terms of local and global parameters.

The existing speckle pattern fabrication techniques documented in the literature can satisfy the requirements in most common experimental conditions. However, for some special and extreme cases in practical experiments, speckle pattern fabrication definitely needs further refinement and more studies. These cases include but are not limited to: (1) Extreme high temperature environment (e.g. high temperature wind tunnel) for hypersonic vehicles. In this case, besides air friction and vibration, the speckle pattern has to stand high temperature far beyond 1000°C at wind speed exceeding 5 Mach; (2) Underwater or marine environment. The speckle patterns need to stand the moisture and corrosion; (3) In-situ long-term creep strain monitoring in out-door conditions or for creep damage evaluation in power plant steels. In these cases, speckle patterns are required to stand for moisture, high-temperature, oxidation for long duration; Furthermore, the inexpensive and more practical micro- and nano-sized pattern fabrication at elevated temperature requires further studying to facilitate research on the crack propagation behavior, crack tip estimation, microstructure deformation observation by SEM imaging and other high magnification optical imaging at high temperatures.

Fig. 8 Mean bias error and standard deviation error of measured u-displacement as a function of sub-pixel displacement



Acknowledgements This work is supported by National Natural Science Foundation of China (NSFC) (Grant nos. 11272032, 11322220, 11427802, 11602011 and 11632010), and the Aeronautical Science Foundation of China (2016ZD51034), and Beijing Nova Program (xx2014B034).

References

- Peters WH, Ranson WF (1981) Digital imaging techniques in experimental stress analysis. *Opt Eng* 21:427–431
- Chu TC, Ranson WF, Sutton MA (1985) Applications of digital-image-correlation techniques to experimental mechanics. *Exp Mech* 25(3):232–244
- Sutton MA, Mingqi C, Peters WH, Chao YJ, McNeill SR (1986) Application of an optimized digital correlation method to planar deformation analysis. *Image Vis Comput* 4(3):143–150
- Peters WH, Ranson WF, Sutton MA, Chu TC, Anderson J (1983) Application of digital correlation methods to rigid body mechanics. *Opt Eng* 22(6):738–742
- Sutton MA, Orteu J, Schreier HW (2009) *Image correlation for shape, motion and deformation measurements*. Springer, US
- Pan B, Qian K, Xie HM, Asundi A (2009) Two-dimensional digital image correlation for in-plane displacement and strain measurement: a review. *Meas Sci Tech* 20(6):062001
- Pan B (2011) Recent progress in digital image correlation. *Exp Mech* 51(7):1223–1235
- Zhou P, Goodson KE (2001) Subpixel displacement and deformation gradient measurement using digital image/speckle correlation (DISC). *Opt Eng* 40(8):1613–1620
- Lecompte D, Smits A, Bossuyt S, Sol H, Vantomme J, Van Hemelrijck D, Habraken AM (2006) Quality assessment of speckle patterns for digital image correlation. *Opt Lasers Eng* 44(11):1132–1145
- Sun YF, Pang HJ (2007) Study of optimal subset size in digital image correlation of speckle pattern images. *Opt Lasers Eng* 45:967–974
- Pan B, Xie HM, Wang ZY, Qian KM, Wang ZY (2008) Study on subset size selection in digital image correlation for speckle patterns. *Opt Exp* 16(10):7037–7048
- Wang YQ, Sutton MA, Bruch HA, Schreier HW (2009) Quantitative error assessment in pattern matching: effects of intensity pattern noise, interpolation, strain and image contrast on motion measurement. *Strain* 45:160–178
- Pan B, Lu ZX, Xie HM (2010) Mean intensity gradient: an effective global parameter for quality assessment of the speckle patterns used in digital image correlation. *Opt Lasers Eng* 48(4):469–477
- Hua T, Xie H, Wang S, Hu Z, Chen P, Zhang Q (2011) Evaluation of the quality of a speckle pattern in the digital image correlation method by mean subset fluctuation. *Opt Laser Technol* 43(1):9–13
- Stoilov G, Kavardzhikov V, Pashkouleva D (2012) A comparative study of random patterns for digital image correlation. *J Theo Appl Mech* 42(2):55–66
- Crammond G, Boyd SW, Dulieu-Barton JM (2013) Speckle pattern quality assessment for digital image correlation. *Opt Lasers Eng* 51(12):1368–1374
- Bossuyt S (2013) Optimized patterns for digital image correlation. In: *Imaging methods for novel materials and challenging applications*, vol 3. Springer, New York, pp 239–248
- Liu XY, Li RL, Zhao HW, Cheng TH, Cui GJ, Tan QC, Meng GW (2015) Quality assessment of speckle patterns for digital image correlation by Shannon entropy. *Opt Int J Light Electron Opt* 126(23):4206–4211
- Mazzoleni P, Zappa E, Matta F, Sutton MA (2015) Thermo-mechanical toner transfer for high-quality digital image correlation speckle patterns. *Opt Lasers Eng* 75:72–80
- Negggers J, Blaysat B, Hoefnagels JPM, Geers MGD (2016) On image gradients in digital image correlation. *Int J Num Meth Eng* 105(4):243–260
- Bomarito GF, Hochhalter JD, Ruggles TJ, Cannon AH (2017) Increasing accuracy and precision of digital image correlation through pattern optimization. *Opt Lasers Eng* 91:73–75
- Luo PF, Chao YJ, Sutton MA, Peters WH (1993) Accurate measurement of three-dimensional deformations in deformable and rigid bodies using computer vision. *Exp Mech* 33(2):123–132
- Helm JD, McNeill SR, Sutton MA (1996) Improved three-dimensional image correlation for surface displacement measurement. *Opt Eng* 35(7):1911–1920
- Pan B, Wu DF, Yu LP (2012) Optimization of a three-dimensional digital image correlation system for deformation measurement in extreme environments. *App Opt* 51(19):4409–4419
- Bay BK, Smith TS, Fyhrig DP, Saad M (1999) Digital volume correlation: three-dimensional strain mapping using X-ray tomography. *Exp Mech* 39(3):217–226
- Pan B, Wu DF, Wang ZY (2012) Internal displacement and strain measurement using digital volume correlation: a least squares framework. *Meas Sci Tech* 23:045002
- Li XD, Xu WJ, Sutton MA, Mello M (2007) *In situ* nanoscale in-plane deformation studies of ultrathin polymeric films during tensile deformation using atomic force microscopy and digital image correlation techniques. *Nanotechnology* 16(1):4–13
- Sachs C, Fabritius H, Raabe D (2006) Experimental investigation of the elastic–plastic deformation of mineralized lobster cuticle by digital image correlation. *J Struct Bio* 155(3):409–425
- Sutton MA, Ke X, Lessner SM, Goldbach M, Yost M, Zhao F, Schreier HW (2008) Strain field measurements on mouse carotid arteries using microscopic three-dimensional digital image correlation. *J Bio Mater Res A* 84(1):178–190
- Ouglova A, Berthaud Y, Focf F, François M, Ragueneau F, Petre-Lazar I (2008) The influence of corrosion on bond properties between concrete and reinforcement in concrete structures. *Mater Struct* 41(5):969–980
- Pan B, Xie HM, Hua T, Asundi A (2009) Measurement of coefficient of thermal expansion of films using digital image correlation method. *Polym Test* 28(1):75–83
- Schreier HW, Garcia D, Sutton MA (2004) Advances in light microscope stereo vision. *Exp Mech* 44(3):278–288
- Guo SM, Sutton MA, Majumdar P, Reifsnider KM, Yu L, Gresil M (2014) Development and application of an experimental system for the study of thin composites undergoing large deformations in combined bending–compression loading. *J Comp Mater* 48(8):997–1023
- Murasawa G, Yoneyama S, Sakuma T (2007) Nucleation, bifurcation and propagation of local deformation arising in NiTi shape memory alloy. *Smart Mater Struct* 16(1):160–167
- Grant BMB, Stone HJ, Withers PJ, Preuss M (2009) High temperature strain field measurement using digital image correlation. *J Strain Anal Eng Des* 44:263–271
- Pan B, Wu D, Xia Y (2010) High-temperature deformation field measurement by combining transient aerodynamic heating simulation system and reliability-guided digital image correlation. *Opt Lasers Eng* 48:841–848
- Dong Y, Hideki K, Yutaka K (2014) Optical system for microscopic observation and strain measurement at high temperature. *Meas Sci Technol* 25(2):025002
- Banks J, Giovannetti LM, Soubeyran X, Wright AM, Turnock SR, Boyd SW (2015) Assessment of digital image correlation as a method of obtaining deformations of a structure under fluid load. *J Fluid Struct* 58:173–187

39. Pan B, Yu LP, Wu DF (2015) Thermo-mechanical response of superalloy honeycomb sandwich panels subjected to non-steady thermal loading. *Mater Des* 88:528–536
40. Reu P (2014) All about speckles: speckle size measurement. *Exp Tech* 38(6):1–2
41. Reu P (2015) All about speckles: speckle density. *Exp Tech* 39(3):1–2
42. Reu P (2015) All about speckles: contrast. *Exp Tech* 39(1):1–2
43. Reu P (2014) All about speckles: aliasing. *Exp Tech* 38(5):1–3
44. Reu P (2015) All about speckles: edge sharpness. *Exp Tech* 39(2):1–2
45. Bruck HA, McNeill SR, Sutton MA, Peters WH (1989) Digital image correlation using Newton–Raphson method of partial differential correction. *Exp Mech* 29:261–267
46. Pan B, Xie HM, Xu BQ, Dai FL (2006) Performance of sub-pixel registration algorithms in digital image correlation. *Meas Sci Tech* 17(6):1615–1621
47. Pan B, Li K (2011) A fast digital image correlation method for deformation measurement. *Opt Lasers Eng* 49(7):841–847
48. Pan B, Li K, Tong W (2013) Fast, robust and accurate digital image correlation calculation without redundant computations. *Exp Mech* 53(7):1277–1289
49. Pan B, Tian L, Song X (2016) Real-time, non-contact and targetless measurement of vertical deflection of bridges using off-axis digital image correlation. *NDT & E Int* 79:73–80
50. Pan B, Wang B (2016) Digital image correlation with enhanced accuracy and efficiency: a comparison of two subpixel registration algorithms. *Exp Mech* 56(8):1395–1409
51. Pan B (2014) An evaluation of convergence criteria for digital image correlation using inverse compositional gauss–Newton algorithm. *Strain* 50(1):48–56
52. Sánchez-Arévalo FM, Pulos G (2008) Use of digital image correlation to determine the mechanical behavior of materials. *Mater Charact* 59(11):1572–1579
53. Gauvin C, Jullien D, Doumalin P, Dupré JC, Gril J (2014) Image correlation to evaluate the influence of hygrothermal loading on wood. *Strain* 50(5):428–435
54. Bourcier M, Bornert M, Dimanov A, Héripré E, Raphanel JL (2013) Multiscale experimental investigation of crystal plasticity and grain boundary sliding in synthetic halite using digital image correlation. *J Geophys Res: Solid Earth* 118(2):511–526
55. Hall SA, Bornert M, Desrues J, Pannier Y, Lenoir N, Viggiani G, Bésuelle P (2010) Discrete and continuum analysis of localized deformation in sand using X-ray μ CT and volumetric digital image correlation. *Geotechnique* 60(5):315–322
56. Wang Y, Cuitiño AM (2002) Full-field measurements of heterogeneous deformation patterns on polymeric foams using digital image correlation. *Int J of Sol and Struc* 39(13):3777–3796
57. Rae PJ, Palmer SJP, Goldrein HT, Lewis AL, Field JE (2004) White-light digital image cross-correlation (DICC) analysis of the deformation of composite materials with random microstructure. *Opt Lasers Eng* 41(4):635–648
58. Jin H, Bruck HA (2005) A new method for characterizing nonlinearity in scanning probe microscopes using digital image correlation. *Nanotechnology* 16(9):1849–1855
59. Srinivasan V, Radhakrishnan S, Zhang X, Subbarayan G, Baughn T, Nguyen L (2005) High resolution characterization of materials used in packages through digital image correlation. ASME pacific rim technical conference and exhibition on integration and packaging of MEMS, NEMS, and electronic systems collocated with the ASME 2005 heat transfer summer conference pp1471–1478
60. Zhang D, Luo M, Arola DD (2006) Displacement/strain measurements using an optical microscope and digital image correlation. *Opt Eng* 45(3): 033605-033605-9
61. Jin H, Lu WY, Korellis J (2008) Micro-scale deformation measurement using the digital image correlation technique and scanning electron microscope imaging. *J Strain Anal Eng* 43(8):719–728
62. Sjögren T, Persson PE, Vomacka P (2011) Analysing the deformation behaviour of compacted graphite cast irons using digital image correlation techniques. *Key Eng Mater Trans Tech Publications* 457:470–475
63. Ghadbeigi H, Pinna C, Celotto S (2012) Quantitative strain analysis of the large deformation at the scale of microstructure: comparison between digital image correlation and microgrid techniques. *Exp Mech* 52(9):1483–1492
64. Dusserre G, Nazaret F, Robert L, Cutard T (2013) Applicability of image correlation techniques to characterise asymmetric refractory creep during bending tests. *J Eur Ceram Soc* 33(2):221–231
65. Su YQ, Yao XF, Wang S, Ma YJ (2015) Improvement on measurement accuracy of high-temperature DIC by grayscale-average technique. *Opt Lasers Eng* 75:10–16
66. Xiong H, Li S, Xiao T (2015) A scheme of deformation measurement for cancellous bones based on the digital image correlation method. 8th international conference on biomedical engineering and informatics (BMEI) IEEE pp 391–396
67. Zhang X, Wang Y, Yang J, Qiao Z, Ren C, Chen C (2016) Deformation analysis of ferrite/pearlite banded structure under uniaxial tension using digital image correlation. *Opt Lasers Eng* 85:24–28
68. Turner JL, Russell SS (1990) Application of digital image analysis to strain measurement at elevated temperature. *Strain* 26(2):55–59
69. Meyer P, Waas AM (2015) Measurement of *in situ*-full-field strain maps on ceramic matrix composites at elevated temperature using digital image correlation. *Exp Mech* 55(5):795–802
70. Brillaud J, Lagattu F (2002) Limits and possibilities of laser speckle and white-light image-correlation methods: theory and experiments. *Appl Opt* 41:6603–6613
71. Lyons JS, Liu J, Sutton MA (1996) High-temperature deformation measurements using digital-image correlation. *Exp Mech* 36(1):64–70
72. Walley JL, Wheeler R, Uchic MD, Mills MJ (2012) In-situ mechanical testing for characterizing strain localization during deformation at elevated temperatures. *Exp Mech* 52(4):405–416
73. Kammers AD, Daly S (2011) Small-scale patterning methods for digital image correlation under scanning electron microscopy. *Meas Sci Technol* 22(12):125501
74. Sutton MA, Li N, Joy DC, Reynolds AP, Li X (2007) Scanning electron microscopy for quantitative small and large deformation measurements part I: SEM imaging at magnifications from 200 to 10,000. *Exp Mech* 47(6):775–787
75. Jonnalagadda KN, Chasiotis I, Yagnamurthy S, Lambros J, Pulskamp J, Polcawich R, Dubey M (2010) Experimental investigation of strain rate dependence of nanocrystalline Pt films. *Exp Mech* 50(1):25–35
76. Winiarski B, Schajer GS, Withers PJ (2012) Surface decoration for improving the accuracy of displacement measurements by digital image correlation in SEM. *Exp Mech* 52(7):793–804
77. Dong Y, Kakisawa H, Kagawa Y (2015) Development of micro-scale pattern for digital image correlation up to 1400 °C. *Opt Lasers Eng* 68:7–15
78. Stinville JC, Echlin MP, Texier D, Bridier F, Bocher P, Pollock TM (2016) Sub-grain scale digital image correlation by electron microscopy for polycrystalline materials during elastic and plastic deformation. *Exp Mech* 56(2):197–216
79. Lionello G, Cristofolini L (2014) A practical approach to optimizing the preparation of speckle patterns for digital-image correlation. *Meas Sci Tech* 25(10):107001
80. Abdellah A, Baierl D, Fabel B, Lugli P, Scarpa G (2009) Spray-coating deposition for large area organic thin-film devices. *NSTI-Nanotech* 2:447–445



81. Rayan MK (2008) Spray deposition of biomolecular thin films. Dissertation, University of South Florida
82. Liu J, Sutton M, Lyons J, Deng X (1998) Experimental investigation of near crack tip creep deformation in alloy 800 at 650 °C. *Int J Frac* 91(3):233–268
83. Pan B, Wu DF, Wang ZY, Xia Y (2011) High-temperature digital image correlation for full-field deformation measurement at 1200 °C. *Meas Sci Technol* 22(1):015701
84. Novak MD, Zok FW (2011) High-temperature materials testing with full-field strain measurement: experimental design and practice. *Rev Sci Instrum* 82:115101
85. Pan B, Wu D, Gao J (2013) High-temperature strain measurement using active imaging digital image correlation and infrared radiation heating. *J Strain Anal Eng Des* 0309324713502201
86. Lyons J, Sutton M, Reynolds A (1998) Experimental characterization of crack tip deformation fields in alloy 718 at high temperatures. *J Eng Mater Tech* 120(1):71–78
87. Sharma SK, Ko GD, Kang KJ (2009) High temperature creep and tensile properties of alumina formed on ferroalloy foils doped with yttrium. *J Eur Ceram Soc* 29(3):355–362
88. De Strycker M, Schueremans L, Van Paeppegem W, Debruyne D (2010) Measuring the thermal expansion coefficient of tubular steel specimens with digital image correlation techniques. *Opt Lasers Eng* 48(10):978–986
89. Leplay P, Réthoré J, Meille S, Baietto MC (2012) Identification of asymmetric constitutive laws at high temperature based on digital image correlation. *J Eur Ceram Soc* 32(15):3949–3958
90. Pan B, Jiang T, Wu D (2014) Strain measurement of objects subjected to aerodynamic heating using digital image correlation: experimental design and preliminary results. *Rev Sci Instr* 85(11):115102
91. Hammer JT, Seidt JD, Gilat A (2014) Strain measurement at temperatures up to 800 °C utilizing digital image correlation. *Adv of Opt Methods Exp Mech* 3:167–170
92. Berke RB, Lambros J (2014) Ultraviolet digital image correlation (UV-DIC) for high temperature applications. *Rev Sci Instr* 85(4):045121
93. Appleby MP, Zhu D, Morscher GN (2015) Mechanical properties and real-time damage evaluations of environmental barrier coated SiC/SiC CMCs subjected to tensile loading under thermal gradients. *Sur Coat Technol* 284:318–326
94. Leplay P, Lafforgue O, Hild F (2015) Nalysis of asymmetrical creep of a ceramic at 1350 °C by digital image correlation. *J Ame Cera Soc* 98(7):2240–2247
95. Chen L, Wang Y, Dan X, Xiao Y, Yang L (2016) Experimental research of digital image correlation system in high temperature test. Seventh international symposium on precision mechanical measurements. *Intern Soc opt photo*, 990306-990306-8
96. Berfield TA, Patel JK, Shimmin RG, Braun PV, Lambros J, Sottos NR (2007) Micro-and nanoscale deformation measurement of surface and internal planes via digital image correlation. *Exp Mech* 47(1):51–62
97. Niendorf T, Burs C, Canadinc D, Maier HJ (2009) Early detection of crack initiation sites in TiAl alloys during low-cycle fatigue at high temperatures utilizing digital image correlation. *Int J Mater Res* 100(4):603–608
98. Thompson MS, Schell H, Lienau J, Duda GN (2007) Digital image correlation: a technique for determining local mechanical conditions within early bone callus. *Med Eng Phys* 29(7):820–823
99. Zhang D, Arola DD (2004) Applications of digital image correlation to biological tissues. *J Biomed Opt* 9(4):691–699
100. Lauret C, Hrapko M, Van Dommelen JAW et al (2009) Optical characterization of acceleration-induced strain fields in inhomogeneous brain slices. *Med Eng Phys* 31(3):392–399
101. Kelleher JE, Zhang K, Siegmund T, Chan RW (2010) Spatially varying properties of the vocal ligament contribute to its eigen frequency response. *J Mech Behav Biomed Mater* 3:600–609
102. Myers KM, Coudrillier B, Boyce BL, Nguyen TD (2010) The inflation response of the posterior bovine sclera. *Acta Biomater* 6:4327–4335
103. Ahn B, Kim J (2010) Measurement and characterization of soft tissue behavior with surface deformation and force response under large deformations. *Med Image Anal* 14:138–148
104. Yamaguchi H, Kikugawa H, Asaka T, Kasuya H, Kuninori M (2011) Measurement of cortical bone strain distribution by image correlation techniques and from fracture toughness. *Mater Trans* 52:1026–1032
105. Brunon A, Bruyère-Gamier K, Coret M (2011) Characterization of the nonlinear behaviour and the failure of human liver capsule through inflation tests. *J Mech Behav Biomed Mater* 4:1572–1581
106. Tiozzi R, Lin L, Rodrigues RC, Heo YC, Conrad HJ, de Mattos MG, Ribeiro RF, Fok AS (2011) Digital image correlation analysis of the load transfer by implant-supported restorations. *J Biomech* 44:1008–1013
107. Libertiaux V, Pascon F, Cescotto S (2011) Experimental verification of brain tissue incompressibility using digital image correlation. *J Mech Behav Biomed Mater* 4(7):1177–1185
108. Soons J, Lava P, Debruyne D, Dirckx J (2012) Full-field optical deformation measurement in biomechanics: digital speckle pattern interferometry and 3D digital image correlation applied to bird beaks. *J Mech Behav Biomed Mater* 14:186–191
109. Ottenio M, Tran D, Annaidh AN, Gilchrist MD, Bruyère K (2015) Strain rate and anisotropy effects on the tensile failure characteristics of human skin. *J Mech Behav Biomed Mater* 41:241–250
110. Palanca M, Brugo TM, Cristofolini L (2015) Use of digital image correlation to investigate the biomechanics of the vertebra. *J Mech Med Bio* 15(02):1540004
111. Zhou B, Ravindran S, Ferdous J, Kidane A, Sutton MA, Shazly T (2016) Using digital image correlation to characterize local strains on vascular tissue specimens. *J Vis Exp* 107:e53625. doi:10.3791/53625
112. Hu Z, Luo H, Du Y, Lu H (2013) Fluorescent stereo microscopy for 3D surface profilometry and deformation mapping. *Opt Exp* 21(10):11808–11818
113. LePage WS, Daly SH, Shaw JA (2016) Cross polarization for improved digital image correlation. *Exp Mech* 56(6):969–985
114. Emsile AG, Bonner FT, Peek LG (1958) Flow of a viscous liquid on a rotating disk. *J Appl Phys* 29:858–862
115. Sahu N, Parija B, Panigrahi S (2009) Fundamental understanding and modeling of spin coating process: a review. *Indian J Phys* 83(4):493–502
116. Tyona MD (2013) A theoretical study on spin coating technique. *Adv Mater Res* 2(4):195–208
117. Wang H, Xie H, Li Y, Zhu J (2012) Fabrication of micro-scale speckle pattern and its applications for deformation measurement. *Meas Sci Technol* 23(3):035402
118. Berfield TA, Patel JK, Shimmin RG, Braun PV, Lambros J, Sottos NR (2006) Fluorescent image correlation for nanoscale deformation measurements. *Small* 2(5):631–635
119. Berfield TA, Carroll JF III, Payne DA et al (2009) Thermal strain measurement in sol-gel lead zirconate titanate thin films. *J Appl Phys* 106(12):123501
120. Hamilton AR, White SR, Sottos NR (2007) Characterization of microvascular networks for self-healing using fluorescent digital image correlation. Proceedings of the first international conference on self healing materials 18-20 April, Noordwijk aan zee, The Netherlands
121. Wilhelmssen AN (2015) Characterization of local strain fields in cross-ply composites under transverse loading. Dissertation, University of Illinois, Urbana-Champaign

122. Carroll J, Abuzaid W, Lambros J, Sehitoglu H (2010) An experimental methodology to relate local strain to microstructural texture. *Rev Sci Instrum* 81(8):083703
123. Karanjgaokar NJ, Oh CS, Chasiotis I (2011) Microscale experiments at elevated temperatures evaluated with digital image correlation. *Exp Mech* 51(4):609–618
124. Padilla HA, Lambros J, Beaudoin AJ, Robertson IM (2012) Relating inhomogeneous deformation to local texture in zirconium through grain-scale digital image correlation strain mapping experiments. *International Journal of Solids and Structures* In *J Solids Struct* 49(1):18–31
125. Casperon MC, Carroll JD, Lambros J, Sehitoglu H, Dodds RH (2014) Investigation of thermal effects on fatigue crack closure using multiscale digital image correlation experiments. *Int J Fatigue* 61:10–20
126. Pataky GJ, Sehitoglu H (2015) Experimental methodology for studying strain heterogeneity with microstructural data from high temperature deformation. *Exp Mech* 55(1):53–63
127. Luo Y, Ruff J, Ray R, Gu Y, Ploehn HJ, Scrivens WA (2005) Vapor-assisted remodeling of thin gold films. *Chem Mater* 17(20):5014–5023
128. Scrivens WA, Luo Y, Sutton MA et al (2007) Development of patterns for digital image correlation measurements at reduced length scales. *Exp Mech* 47(1):63–77
129. Li N, Sutton MA, Li X, Schreier HW (2008) Full-field thermal deformation measurements in a scanning electron microscope by 2D digital image correlation. *Exp Mech* 48(5):635–646
130. Di Gioacchino F, da Fonseca JQ (2013) Plastic strain mapping with sub-micron resolution using digital image correlation. *Exp Mech* 53(5):743–754
131. McCord MA, Rooks MJ (1997) Electron beam lithography. *Handbook of Microlithography, Micromachining, and Microfabrication* 1:139–249
132. Seal S (Ed.) (2010) *Functional nanostructures: processing, characterization, and applications*. Springer Science & Business Media
133. Sutton MA, Zhao W, McNeill SR, Helm JD, Piascik RS, Riddell WT (1999) local crack closure measurements: development of a measurement system using computer vision and a far-field microscope. In *advances in fatigue crack closure measurement and analysis*, vol 2, ASTM International
134. Zhang Y, Topping TD, Lavernia EJ, Nutt SR (2014) Dynamic micro-strain analysis of ultrafine-grained aluminum magnesium alloy using digital image correlation. *Metall Mater Trans A* 45(1):47–54
135. Latourte F, Salez T, Guery A, Rupin N, Mahe M (2014) Deformation studies from *in situ* SEM experiments of a reactor pressure vessel steel at room and low temperatures. *J Nuc Mater* 454(1):373–380
136. Allais L, Bornert M, Bretheau T, Caldemaison D (1994) Experimental characterization of the local strain field in a heterogeneous elastoplastic material. *Acta Metall et Mater* 42(11):3865–3880
137. Guery A, Latourte F, Hild F, Roux S (2013) Characterization of SEM speckle pattern marking and imaging distortion by digital image correlation. *Meas Sci Tech* 25(1):015401
138. Li N, Guo S, Sutton MA (2011) Recent progress in e-beam lithography for SEM patterning. In *MEMS and Nanotechnology*, 2, Springer, New York, pp 163–166
139. Tanaka Y, Naito K, Kishimoto S, Kagawa Y (2011) Development of a pattern to measure multiscale deformation and strain distribution via *in situ* FE-SEM observations. *Nanotechnology* 22(11):115704
140. Carter JLW, Uchic MD, Mills MJ (2015) Impact of speckle pattern parameters on DIC strain resolution calculated from in-situ SEM experiments. In *fracture, fatigue, failure, and damage evolution*, 5, Springer, pp 119–126
141. Melngailis J (1987) Focused ion beam technology and applications. *J Vac Sci Technol B* 5(2):469–495
142. Liu Z, Xie H, Fang D et al (2007) Deformation analysis in microstructures and micro-devices. *Microelec Reliab* 47(12):2226–2230
143. Korsunsky A, Sebastiani M, Bemporad E (2009) Focused ion beam ring drilling for residual stress evaluation. *Mater Lett* 63:1961–1963
144. Sebastiani M, Eberl C, Bemporad E, Pharr GM (2011) Depth-resolved residual stress analysis of thin coatings by a new FIB-DIC method. *Mater Sci Eng A* 528(27):7901–7908
145. Li Y, Xie HM, Wang QH, Liu ZW (2013) Fabrication technique of deformation carriers (gratings and speckle patterns) with FIB for microscale/nanoscale deformation measurement. *FIB Nanostructures*, Springer, pp 267–298
146. Sabate N, Vogel D, Gollhardt A, Marcos J, Gracia I, Cane C, Michel B (2006) Digital image correlation of nanoscale deformation fields for local stress measurement in thin films. *Nanotechnology* 17:5264–5270
147. Winiarski B, Withers PJ (2012) Micron-scale residual stress measurement by micro-hole drilling and digital image correlation. *Exp Mech* 52(4):417–428
148. Zhu R, Xie H, Xue Y, Wang L, Li Y (2015) Fabrication of speckle patterns by focused ion beam deposition and its application to micro-scale residual stress measurement. *Meas Sci Technol* 26(9):095601
149. Thompson RJ, Hemker KJ (2007) Thermal expansion measurements on coating materials by digital image correlation. *Proceedings of the 2007 SEM annual conference and exposition on exposition on experimental and applied mechanics*. Springfield, Massachusetts
150. Blaber J, Adair BS, Antoniou A (2015) A methodology for high resolution digital image correlation in high temperature experiments. *Rev Sci Instrum* 86(3):035111
151. Biery NE, De Graef M, Pollock TM (2001) Influence of microstructure and strain distribution on failure properties in intermetallic TiAl-based alloys. *Mater Sci Eng A*, 319–321: 613–617
152. Biery N, De Graef M, Pollock TM (2003) A method for measuring microstructural-scale strains using a scanning electron microscope: applications to γ -titanium aluminides. *Metall Mater Trans A* 34(10):2301–2313
153. Zink AG, Davidson RW, Hanna RB (2007) Strain measurement in wood using a digital image correlation technique. *Wood Fiber Sci* 27(4):346–359
154. Helm JD (2008) Digital image correlation for specimens with multiple growing cracks. *Exp Mech* 48(6):753–762
155. Ma J, Goble K, Smietana M, Kostrominova T, Larkin L, Arruda EM (2009) Morphological and functional characteristics of three-dimensional engineered bone-ligament-bone constructs following implantation. *J Biomech Eng* 131(10):101017
156. Avitabile P, Niezrecki C, Helfrick M, Warren C, Pingle P (2010) Noncontact measurement techniques for model correlation. *TEST* 44(2):8–12
157. Jerabek M, Major Z, Lang RW (2010) Strain determination of polymeric materials using digital image correlation. *Polym Test* 29(3):407–416
158. Hisley DM, Gurganus JC, Drysdale AW (2011) Experimental methodology using digital image correlation to assess ballistic helmet blunt trauma. *J Appl Mech* 78(5):051022
159. Castelluccio GM, Yawny AA, Perez Ipina JE et al (2012) *In situ* evaluation of tensile properties of heat-affected zones from welded steel pipes. *Strain* 48(1):68–74
160. Kammers AD, Daly S (2013) Self-assembled nanoparticle surface patterning for improved digital image correlation in a scanning electron microscope. *Exp Mech* 53(8):1333–1341



161. Deneweth JM, Newman KE, Sylvia SM, McLean SG, Arruda EM (2013) Heterogeneity of tibial plateau cartilage in response to a physiological compressive strain rate. *J Orthop Res* 31(3):370–375
162. Mahalingam VD, Behbahani-Nejad N, Horine VS, Olsen TJ, Smietana MJ, Wojtys EM, Wellik DM, Arruda EM, Larkin LM (2015) Allogeneic versus autologous derived cell sources for use in engineered bone-ligament-bone grafts in sheep anterior cruciate ligament repair. *Tissue Eng A* 21(5–6):1047–1054
163. Bong WJ, Daly S, Shorter KA. Full field *in vivo* characterization of skin deformation under pressure loading
164. Williams GM, Gratz KR, Sah RL (2009) Asymmetrical strain distributions and neutral axis location of cartilage in flexure. *J Biomech* 42(3):325–330
165. Cannon AH, Hochhalter JD, Mello AW, Bomarito GF, Sangid MD (2015) Micro stamping for improved speckle patterns to enable digital image correlation. *Microsc Microanal* 21(S3):451–452
166. Hung PC, Voloshin AS (2003) In-plane strain measurement by digital image correlation. *J Braz Soc Mech Sci Eng* 25(3):215–221
167. Gates M, Gonzalez J, Lambros J, Heath MT (2015) Subset refinement for digital volume correlation: numerical and experimental applications. *Exp Mech* 55(1):245–259